Science of the Total Environment 913 (2024) 169586

Contents lists available at ScienceDirect

Science of the Total Environment

journal homepage: www.elsevier.com/locate/scitotenv

Improved estimation of CO_2 emissions from thermal power plants based on OCO-2 XCO_2 retrieval using inline plume simulation

Yingsong Li [a], Fei Jiang [a,d,e,*], Mengwei Jia [a], Shuzhuang Feng [a], Yong Lai [b], Junnan Ding [c], Wei He [a], Hengmao Wang [a], Mousong Wu [a], Jun Wang [a], Fanhui Shen [f], Lingyu Zhang [a]

[a] Jiangsu Provincial Key Laboratory of Geographic Information Science and Technology, International Institute for Earth System Science, Nanjing University, Nanjing 210023, China
[b] Zhejiang Hangzhou Ecological and Environmental Monitoring Center, Hangzhou 310012, China
[c] China National Environmental Monitoring Centre, Beijing 100012, China
[d] Jiangsu Center for Collaborative Innovation in Geographical Information Resource Development and Application, Nanjing 210023, China
[e] Frontiers Science Center for Critical Earth Material Cycling, Nanjing University, Nanjing 210023, China
[f] National Environmental Protection Research Institute for Electric Power Co., Ltd., Nanjing 210031, China

HIGHLIGHTS

- The estimates of power plant CO_2 emissions have large uncertainties using the simulations of Gaussian plume model.
- Inline plume model can improve the estimates of power plant CO_2 emissions.
- The meteorological field, especially wind speed has a great impact on the inversion results.
- There is a negative correlation between wind speed and plume rise height.

GRAPHICAL ABSTRACT

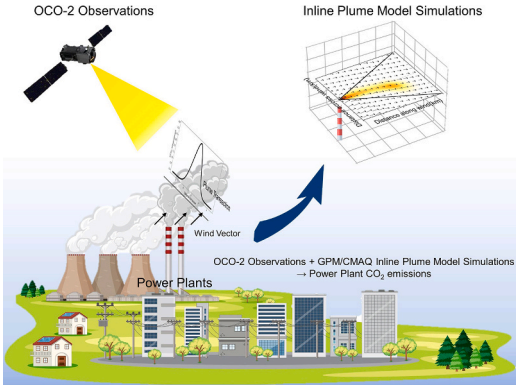

ARTICLE INFO

Editor: Hai Guo

Keywords:
Power plants
CO_2 emissions
WRF-CMAQ model
Gaussian plume model
XCO_2

ABSTRACT

CO_2 emissions from power plants are the dominant source of global CO_2 emissions, thus in the context of global warming, accurate estimation of CO_2 emissions from power plants is essential for the effective control of carbon emissions. Based on the XCO_2 retrievals from the Orbiting Carbon Observatory 2 (OCO-2) and the Gaussian Plume Model (GPM), a series of studies have been carried out to estimate CO_2 emission from power plants. However, the GPM is an ideal model, and there are a number of assumptions that need to be made when using this model, resulting in large uncertainties in the inverted emissions. Here, based on 6 cases of power plant plumes observed by the OCO-2 satellite over the Yangtze River Delta, China, we use an inline plume rise module coupled in the Community Multi-scale Air Quality model (CMAQ) to simulate the plumes and invert the emissions, and compare the simulated plumes and inverted emissions using the GPM model. We found that CO_2

* Corresponding author at: Jiangsu Provincial Key Laboratory of Geographic Information Science and Technology, International Institute for Earth System Science, Nanjing University, Nanjing 210023, China.
E-mail address: jiangf@nju.edu.cn (F. Jiang).

https://doi.org/10.1016/j.scitotenv.2023.169586
Received 21 October 2023; Received in revised form 7 December 2023; Accepted 20 December 2023
Available online 29 December 2023

emissions can be significantly overestimated or underestimated based on the GPM simulations, and that the CMAQ inline plume simulation could significantly improve the estimates. However, the simulation bias in wind speed can significantly affect the inversion results. These results indicate that accurate meteorological field and plume simulations are critical for future inversion of point source emissions.

1. Introduction

CO_2 emissions from coal power plants accounts for 33–40 % of global carbon emissions (Yoro and Daramola, 2020). From the Kyoto Protocol to the Paris Agreement, reducing CO_2 emissions has been constantly emphasized (Razmjoo et al., 2021). In order to achieve this goal and control fossil fuels CO_2 emissions, an accurate estimate for the emissions of coal power plants is particularly important. Traditional estimation methods have high uncertainty in estimating emissions due to the complexity of activity level data and the inaccuracy of emission factors (Friedlingstein et al., 2022). The development of space-based CO_2 observations in recent years, in particular the launch of NASA's Orbiting Carbon Observatory-2 (OCO-2) satellite (Eldering et al., 2017), which provides information on column-averaged CO_2 dry-air mixing ratios (XCO_2) of the CO_2 plume cross-section of power plants (Schwandner et al., 2017), provides a basis for estimating CO_2 emissions through top-down methods.

OCO-2 measures XCO_2 across a narrow swath of about 10 km with a footprint resolution of 1.29 × 2.25 km^2. When it passes through the downwind of an individual point source, the observed XCO_2 is significantly elevated due to strong CO_2 emissions. By fitting the observed XCO_2 to plume simulations, daily CO_2 emissions can be quantified (Nassar et al., 2017). Based on the OCO-2 XCO_2 retrievals, a series of studies have been carried out to estimate CO_2 emissions from power plants, volcanoes, and cities (Guo et al., 2023; Lei et al., 2021; Nassar et al., 2021; Zheng et al., 2020). The Gaussian Plume Model (GPM) is the most widely used model to simulate the smoke plume. Using GPM, Nassar et al. (2021) presented CO_2 emission estimates for twenty power plants and associated facilities in the United States, India, South Africa, Poland, Russia and South Korea, and pointed out that the difference between the estimated and reported emissions for the US power plants ranged from 1.4 % to 26.7 %. Zheng et al. (2020) quantified CO_2 emissions from 46 cities and industrial regions over China. However, Zheng et al. (2019) used the Weather Research and Forecasting model coupled to the Chemistry (WRF-Chem) model alternative GPM to simulate plumes and calculate emissions for 7 cases reported in Nassar et al. (2017), and found that the differences in estimated emissions were more than 50 % in several cases and much lower than the reported emissions. Lin et al. (2023) identified a total of 50 collocated cases of CO_2 emissions involving 22 power plants and found that the instantaneous satellite estimated emissions of these 50 cases and the reported emissions showed a weak correlation. For an identical power plant, the estimated emissions from XCO_2 observations from different dates can differ by a factor of about 7. A possible reason for this situation is that GPM is an idealized plume transport diffusion model, and there are numerous assumptions made when using this model, including the height of the plume rise, atmospheric stability parameters, and so on. In addition, the simulated XCO_2 in the above estimates is usually an average of the CO_2 concentration throughout the whole gas column, whereas the satellite-observed XCO_2 is a weighted average of the different pressure layers. Three-dimensional (3D) atmospheric transport models can more realistically describe atmospheric transport and mixing, thereby better capturing the structure of real plumes (Brunner et al., 2023), and can simulate the vertical profile of CO_2 concentrations, allowing us to calculate simulated XCO_2 based on the average kernel of satellite observations. There have been several studies using 3D atmospheric transport models for plume simulation and inversion of CO_2 emissions at the city scale (Pillai et al., 2016; Broquet et al., 2018; Ye et al., 2020; Lei et al., 2022). Zheng et al. (2019) also employed high-resolution simulations of a 3D atmospheric transport model (i.e., WRF-Chem) to estimate power plant CO_2 emissions. To date, however, there have been few studies that include calculations of plume rise.

The Yangtze River Delta (YRD) region is one of the most economically developed and CO_2 emitting regions in China. There are many thermal power plants here. In order to estimate CO_2 emissions more accurately from power plants, in this study, we used a 3D atmospheric transport model coupled with an in-line plume rise module (i.e., CMAQ) to simulate the plumes and estimate the emissions. To investigate the impacts of the GPM's plume simulations and the calculations of XCO_2 on emission estimates, we also estimated the emissions based on the GPM simulations with the plume rise height outputted from the CMAQ model and the wind field outputted from the WRF model.

2. Data and methods

2.1. The OCO-2 XCO_2 data and selection of power plants in YRD

OCO-2 was launched on July 2, 2014, it flies in a sun-synchronous orbit and passes by ~13:36 local time with a repeat cycle of 16 days (Ng and Hashim, 2023). In this study, we used the OCO-2 ACOS v10 Lite high-quality XCO_2 data filtered by the variable "xco2_quality_flag" from 2017 to 2020. We selected the power plant cases by the following steps: (1) Identifying the coal power plants. The average value of each overpass in YRD was calculated as the background, and the XCO_2 enhancements were calculated by removing the background. If a power plant with reported CO_2 emissions was located within 25 km upwind of OCO-2 overpasses with significant XCO_2 enhancements, the power plant was identified. (2) Accurately calculating the XCO_2 enhancements. To get more accurate XCO_2 enhancements, we re-calculated the background value using the XCO_2 observations along the footprint, and 20–80 km away from the location with the highest XCO_2 concentration. (3) There should be at least 5 soundings with XCO_2 enhancement greater than 1.5 ppm for each identified power plant. Finally, we selected 6 power plant cases. They are Shanghai Wujing Power Station, Jiangsu Nantong Power Station, Zhejiang Jiaxing Power Station, Guohua Taicang Power Station, Huadian Jurong Power Station, and Guoneng Tongling Power Station. The locations of these power plants and the corresponding XCO_2 observations are shown in Fig. 1.

2.2. Meteorological data

Wind speeds from meteorological sites were used to assess the accuracy of the WRF wind speed simulation. The upper air data were obtained from the University of Wyoming (http://weather.uwyo.edu/upperair/bufrraob.shtml, last access: 7 December 2023), which provides the wind speeds of different pressure layers and heights at the sounding site every 12 h. The 10 m wind speeds with a time interval of 1 h or 3 h at the ground-based meteorological observation sites were downloaded from the National Climate Data Center (ftp://ftp.ncdc.noaa.gov/pub/data/noaa/isd-lite/, last access: 6 December 2023). The locations of these sites are shown in Fig. 1(a).

2.3. CO_2 plume simulations

2.3.1. In-line plume simulations

In this study, the WRF-CMAQ model was used to simulate CO_2 inline plume rises and diffusion from power plants. WRF-CMAQ is an offline regional atmospheric chemistry transport model, in which WRF

(Weather Research Forecast) is a new generation of mesoscale forecasting models developed by scientists from many research departments and universities (Skamarock et al., 2019), and CMAQ is a 3D Eulerian atmospheric chemistry and transport simulation system (United States Environmental Protection Agency, 2014). The versions of WRF and CMAQ are 4.0 and 5.0.2, respectively. In the CMAQ v5.0.2, an in-line plume rise simulation module was coupled, in which the atmospheric stability (stable, neutral or unstable) is determined based on the simulated surface heat flux, mixing height and virtual potential temperature gradient variables, etc. Meteorological factors such as wind speed and ambient temperature at the top of the stack, and the stack parameters including stack diameter, stack height, stack exit temperature, and stack exit velocity are used to calculate the effective plume rise height Δh. Then the plume centerline at a given time is equal to the stack height plus Δh. Plume top and plume bottom are defined as the stack height plus 1.5 times Δh and the stack height plus 0.5 times Δh, respectively. Several sections are divided by the model vertical layers between plume bottom and top, and each section at each time step is allocated prior

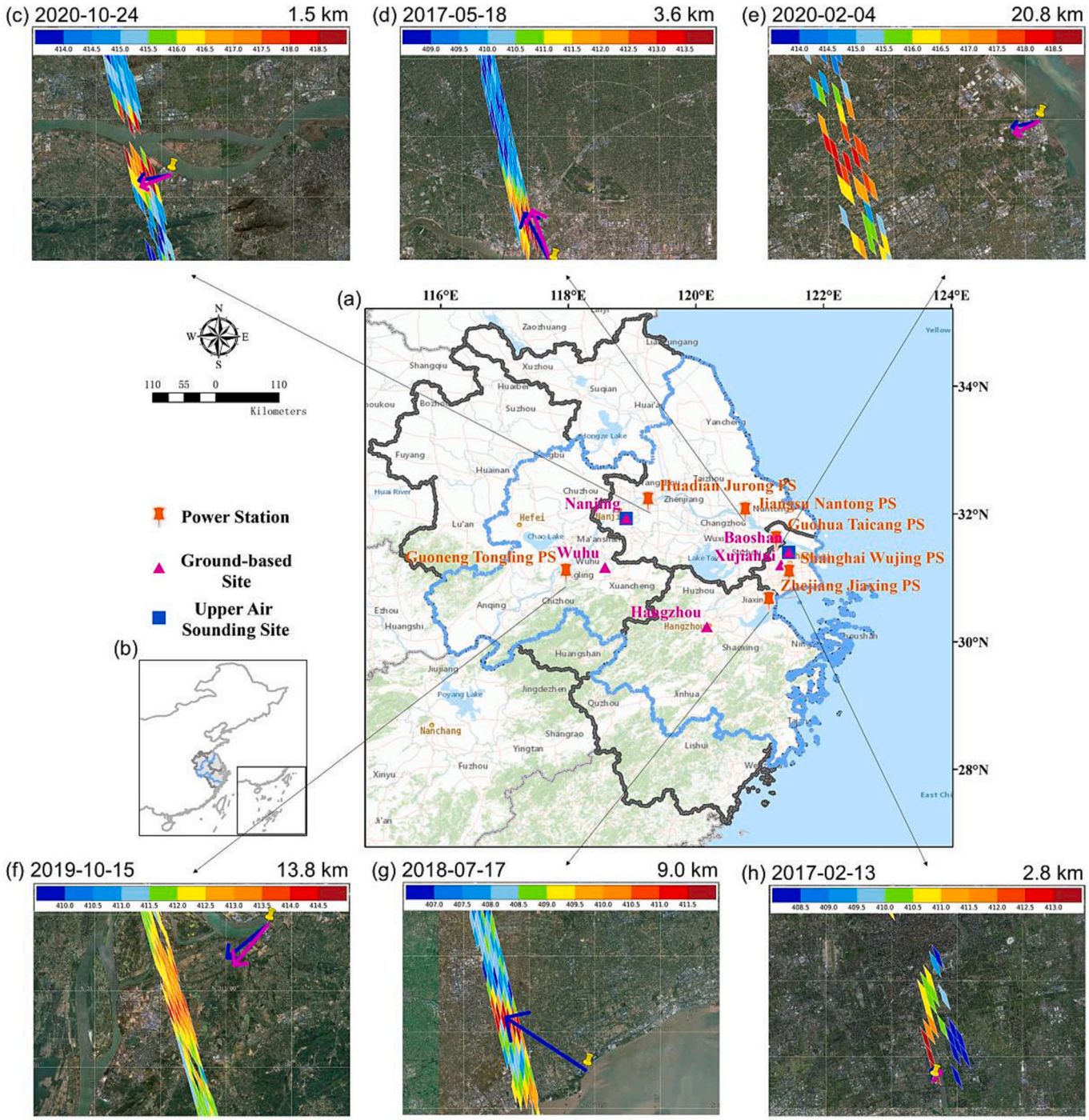

Fig. 1. (a–b) The locations of power plants and meteorological sites in the YRD, and (c-h) the corresponding satellite-based XCO_2 observations in the YRD. (The orange nails indicate the locations of 6 power plants, the rosy triangles represent ground-based meteorological observation sites, the blue squares show upper air meteorological sounding sites, the yellow nails show the locations of the power plants, the rosy arrows are the wind directions at the plume centerline height simulated by WRF, the blue arrows are the optimal wind directions, and the number in the upper right corner is the distance of the power plant from the satellite observation along the optimal wind direction).

emissions in proportion to the plume height (height between the plume bottom and the plume top) it occupies. Finally, the point source prior emissions are assigned between the model layers of the plume top and plume bottom (Bieser et al., 2011; Guevara et al., 2014; Houyoux, 1998; Ooi et al., 2021). In addition, it should be noted that CMAQ is a full chemistry model, that does not contain CO_2 species. In this study, we added a tracer gas of CO_2 and closed the chemical and aerosol processes because there are only advection and diffusion processes for CO_2 in the atmosphere.

According to Brunner et al. (2023), at a resolution of 1 km or higher, the turbulent structure of a plume begins to be resolved. Therefore, for each WRF simulation, we adopted a 4 nested domain, with grid spacing of 27, 9, 3, and 1 km. For each CMAQ simulation, only the domain with 1 km resolution was run. This domain has 97 × 97 grids and we placed the power plant in the center of it. Vertically, there are 51 layers for WRF and 15 layers for CMAQ. For each simulation, WRF was run for 48 h, with start time about 1 day ahead of the OCO-2 satellite transit; and CMAQ was run only on the day of the satellite transit. The initial conditions and boundary conditions of WRF were provided by the final (FNL) operational global analysis data from the National Center for Environmental Prediction, which has a spatial resolution of 1° × 1°, and a temporal interval of 6 h. The initial and lateral boundary conditions of each CMAQ simulation were set to zero, except for the in-line CO_2 emission from one power plant, the other CO_2 fluxes from anthropogenic and natural sources were all set to zero. The stack parameters of the Guohua Taicang Power Station and the Jiangsu Nantong Power Station were from the National Environmental Protection Research Institute for Electric Power Co., Ltd., for the parameters of other power plants, we adopted a default data, namely stack diameter of 8 m, stack height of 210 m, stack exit temperature of 318 K, and stack exit velocity of 22 m/s, which are for power plants with an installed capacity greater than 300 MW. The stack parameters and installed capacity of each power plant in this study are listed in Table 1. For each power plant, we assumed a prior emission rate of 25 $ktCO_2$/day.

Two types of simulated XCO_2 were calculated. The first one is named as weighted XCO_2, which is calculated based on the pressure weighting function and averaging kernel following Connor et al. (2008). The simulated CO_2 concentration profiles were mapped into the satellite XCO_2 retrieval levels and then vertically integrated according to formula (1).

$$X^m_{co_2} = X^a_{co_2} + \sum_j h_j k_j (X_m - X_a)_j \quad (1)$$

where $X^m_{co_2}$ is the modeled XCO_2, $X^a_{co_2}$ is the priori XCO_2, j represents the vertical levels in the OCO-2 Level-2 full-physics retrieval, h_j is the pressure weighting function, k_j is the column averaging kernel, X_m is the simulated CO_2 concentration that has been interpolated to the OCO-2 retrieval pressure levels, and X_a is the priori CO_2 profile. $X^a_{co_2}$, h_j, k_j and X_a are all derived from OCO-2 data products, and the average value of all satellite soundings within the simulated plume is adopted.

We also calculated the column averaged CO_2 concentration using the CMAQ simulations according to O'Dell et al. (2012), which is named as CMAQ averaged XCO_2.

$$X_{co_2} = \frac{\sum_{i=1}^{N-1} \overline{(cu)_i} \Delta p_i}{\sum_{i=1}^{N-1} \overline{c_i} \Delta p_i} \quad (2)$$

$$c \equiv \frac{1-q}{g M_{air}} \quad (3)$$

Where X_{co_2} is the averaged XCO_2, i denotes the model vertical layer, u is the CO_2 concentration, q is the specific humidity, $\overline{(cu)_i}$ and $\overline{c_i}$ means the average of quantity cu and c over layer i, Δp_i is the pressure difference between pressure level p_i and p_{i+1}.

2.3.2. Gaussian plume model

GPM is a normal model based on statistical theory and is mainly used to simulate the diffusion process of emission point sources in the atmosphere (Brusca et al., 2016). The model assumes that the wind speed and direction remain constant during the diffusion process, and that the gas does not settle, decompose, or undergo any chemical reaction during the whole process. GPM simulates XCO_2 enhancement as follows (Bovensmann et al., 2010; Nassar et al., 2021):

$$V(x,y) = \frac{F}{\sqrt{2\pi}\sigma_y(x) u} e^{-\frac{1}{2}\left(\frac{y}{\sigma_y(x)}\right)^2} \quad (4)$$

$$\sigma_y(x) = a \cdot \left(\frac{x}{1000}\right)^{0.894} \quad (5)$$

$$XCO_2 = V(x,y) \cdot \frac{M_{air}}{M_{co_2}} \cdot \frac{g}{P_{surf} - \omega^* g} \bullet 1000 \quad (6)$$

Where $V(x,y)$ is CO_2 vertical column in g/m^2 at the (x,y) position, x is a distance along the optimal wind direction, y is a distance across the optimal wind direction. In Eq. (4), F is the emission rate with a unit of g/s, which needs to be calculated, $\sigma_y(x)$ is the standard deviation in the across-wind direction, and u is the wind speed at the plume centerline height. In this study, u was derived from the WRF simulations according to the plume rise height simulated in the CMAQ in-line plume rise module. In Eq. (5), a is the atmospheric stability parameter, which depends on the surface wind speed, if the surface wind speed is less than 2 m/s, a is 213; if the surface wind speed is greater than 5 m/s, a equals 104; otherwise a is interpolated between 104 and 213. The surface wind speed was also derived from the WRF simulations in this study. The CO_2 vertical column of V is converted to XCO_2 enhancement in ppm according to Eq. (6) (Hu and Shi, 2021; Zheng et al., 2020), where M_{air} and

Table 1
Location, stack parameters and installed capacity for each power plant.

Date	Name	Latitude	Longitude	Stack parameters				Installed capacity (MW)
				Diameter (m)	Height (m)	Exit temperature (K)	Exit velocity (m/s)	
2017/2/13	Shanghai Wujing Power Station	31.061035	121.460165	8	210	318	22	2400
2017/5/18	Jiangsu Nantong Power Station	32.032512	120.771661	8	210	318	22	2700
2018/7/17	Zhejiang Jiaxing Power Station	30.629398	121.146125	8	210	318	22	5000
2019/10/15	Guoneng Tongling Power Station	31.074375	117.964305	8	210	318	22	1200
2020/2/4	Guohua Taicang Power Station	31.584758	121.257726	10	240	318	30	1900
2020/10/24	Huadian Jurong Power Station	32.194023	119.249555	8	210	318	22	4000

M_{co_2} are the mole mass of air and CO_2, and P_{surf} (surface pressure, Pa) and ω (total column water vapor, kg/m^2) were derived from the OCO-2 products.

Following Nassar et al. (2017), we adjusted the wind direction (±45°) at the power plant location to make the correlation coefficient (CORR) between the simulated XCO_2 enhancement and the observed XCO_2 enhancement within the plume diffusion limit (outside which the CO_2 vertical column is less than 1 % of the CO_2 vertical column along the wind direction) reaches the maximum, and finally, the wind direction with the maximum CORR is the optimal wind direction. CORR must be greater than 0.5. For the CMAQ simulations, we used the same plume diffusion limit with GPM, and made a slight shift in the position of the modeled XCO_2 to ensure that the simulated XCO_2 maximum enhancement is located near the observed maximum enhancement.

2.4. Emission inversion and uncertainty estimation

2.4.1. Emission estimation

Based on the simulated and observed XCO_2 enhancement described above, we estimated emissions by the weighted least squares method:

$$\widehat{X} = \left(H^T R^{-1} H\right)^{-1}\left(H^T R^{-1} y\right) \tag{7}$$

$$R[i,j] = \begin{cases} corr(i,j)\cdot\sigma_{xco_{2,i}}\cdot\sigma_{xco_{2,j}(i\neq j)} \\ \sigma_{xco_{2,i}}\cdot\sigma_{xco_{2,j}(i=j)} \end{cases} \tag{8}$$

$$corr(i,j) = \frac{t_{max} - t_{i,j}}{t_{max}} \bullet corr_{max} \tag{9}$$

Where $\widehat{X}$ is the optimal estimated emission rate, H is the XCO_2 enhancement caused by the prior emission per unit. y is the OCO-2 XCO_2 enhancement, and R is a weighting matrix. Following Zheng et al. (2019), R was constructed based on the time relationship between different OCO-2 XCO_2 observations i,j ($corr(i,j)$) and the corresponding retrieval errors of each observation obtained from the OCO-2 product ($\sigma_{xco_{2,i}}$ and $\sigma_{xco_{2,j}}$), $t_{i,j}$ is the observation time difference between footprint i and footprint j. Here, $corr_{max}$ and t_{max} were set to 0.3 and 10 s, respectively.

2.4.2. Uncertainty estimation

Three sources of uncertainty in estimating CO_2 emissions from power plants have been considered in this study. The first one is inversion error (ε_t). According to Zheng et al. (2019), the inversion error is the square root of $\left(H^T R^{-1} H\right)^{-1}$.The second one ($\varepsilon_b$) is caused by the removal of OCO-2 XCO_2 background value. We estimated the emissions with different background XCO_2 values (varied within ±0.1 %), and the standard deviation of the estimated emissions is adopted as this uncertainty. The last uncertainty (ε_w) is caused by the wind speed. The 10 m wind speed is usually overestimated by 0.5–1 m/s over China in WRF (Gao et al., 2016; Zhang et al., 2021). In this study, we evaluate the simulated 10 m wind speeds of WRF using the nearest meteorological data. Since the innermost domain (D04) has a small area of 97 km × 97 km, if there are meteorological stations in the D04 domain, the simulation results of D04 are used for the evaluation, otherwise the simulation results of D03 are used to complete the evaluation. The biases are in the range of −0.31 to 1.7 m/s (see Table S2). Previous studies have typically used 1.3–1.5 times the 10 m wind speed as the upper air wind speed after plume rise (Varon et al., 2018). Therefore, the error of the simulated wind speed at the plume centerline height is about −1.5 to 1.5 m/s. Based on GPM, the emissions with different wind speeds were estimated, and the standard deviation was considered as this uncertainty. In the CMAQ model, we cannot artificially modify the wind speed, the ε_w of emissions based on the CMAQ simulations are scaled according to the relative changes between estimated emission and ε_w using GPM. Many previous studies also considered the plume rise height as another uncertainty source in the inversion (Johnson et al., 2020; Nassar et al., 2021). Since the plume rise height in CMAQ was calculated based on the stack parameters and meteorological conditions on that day, and the same height was used in the GPM, we did not consider this uncertainty. Finally, the three uncertainties were combined according to Eq. (10).

$$\varepsilon = \sqrt{{\varepsilon_t}^2 + {\varepsilon_b}^2 + {\varepsilon_w}^2} \tag{10}$$

3. Results and discussion

3.1. Plume rise height and wind speed

Fig. 2 shows the simulated plume centerline height and corresponding wind speeds at this height for the 6 cases. The maximum plume centerline height reaches about 823 m, while the lowest height is only 310 m. The wind speeds also vary considerably, from a maximum of 11.7 m/s to a minimum of 1.5 m/s. In addition, it can also be found that there is a significant negative correlation between wind speed and plume centerline height, with the plume centerline height being significantly lower when the wind speed is high. After subtracting the stack height, the plume rises between 100 and 613 m. The correlation coefficient between changes in plume rise height and changes in wind speed reaches −0.96 (Fig. 2(b)). In many previous studies, the plume rise was usually assumed to be a typical height (Brunner et al., 2019; Nassar et al., 2017). Obviously, our results show that such an assumption is not reasonable and that the plume rise height must be calculated based on the wind speed.

3.2. Simulated plumes

Fig. 3 shows the simulated distributions of the XCO_2 plumes for the 2020-02-04, 2017-02-13, and 2018-07-17 cases. For comparison, we show the plumes simulated by GPM and calculated using pressure-weighted (Eq. 1) and column-averaged (Eq. 2 and 3) methods based on the CMAQ simulations, which are named as the GPM plume, the CMAQ weighted plume, and the CMAQ averaged plume, respectively. The CMAQ weighted and averaged plumes are basically the same in all the cases, but the CMAQ and GPM plumes differ significantly. Generally, GPM plumes show a half bell-shaped curve along the optimal wind direction, and decrease rapidly along the optimal wind direction. There was a significant difference in the rate of decrease in XCO_2 concentrations with distance at different wind speeds. The lower the wind speed, the faster the rate of decrease in XCO_2. However, in the CMAQ model, wind speed and direction are not fixed but have significant spatial variations, and accordingly, the CMAQ plumes do not follow the optimal wind direction as the GPM plumes do, but rather deflect with the wind field. Meanwhile, the XCO_2 of CMAQ plumes does not always decrease with increasing distance from the stack's location, and at certain specific times such as 2020-02-04, it may appear to decrease and then increase. This may be due to the fact that the plume has a maximum landing point under certain weather conditions, which leads to the accumulation of CO_2 near the maximum landing point. In addition, it can also be noted that closer to the stack, the XCO_2 concentrations of GPM plumes are significantly higher than those of CMAQ plumes.

To further quantify the XCO_2 differences among plumes, we calculated the maximum XCO_2 enhancement along the wind direction (Fig. 4). Clearly, wind speed affects the XCO_2 enhancement, which is more evident at the power plant location. We found that the higher the wind speed, the lower the XCO_2 enhancement at the power plant location. As shown in Fig. 4(b), the wind speed at the plume centerline height was only 1.48 m/s on 2017-02-13. The XCO_2 enhancement at the power plant location for CMAQ weighted, CMAQ averaged, and GPM plumes are 6.90, 6.88, and 24.70 ppm, respectively, while on 2018-07-17 (Fig. 4(c)), the wind speed reaches 11.68 m/s and the XCO_2 enhancement of CMAQ plumes is only about 1 ppm at the power plant location. The XCO_2 enhancement of GPM plumes is also significantly

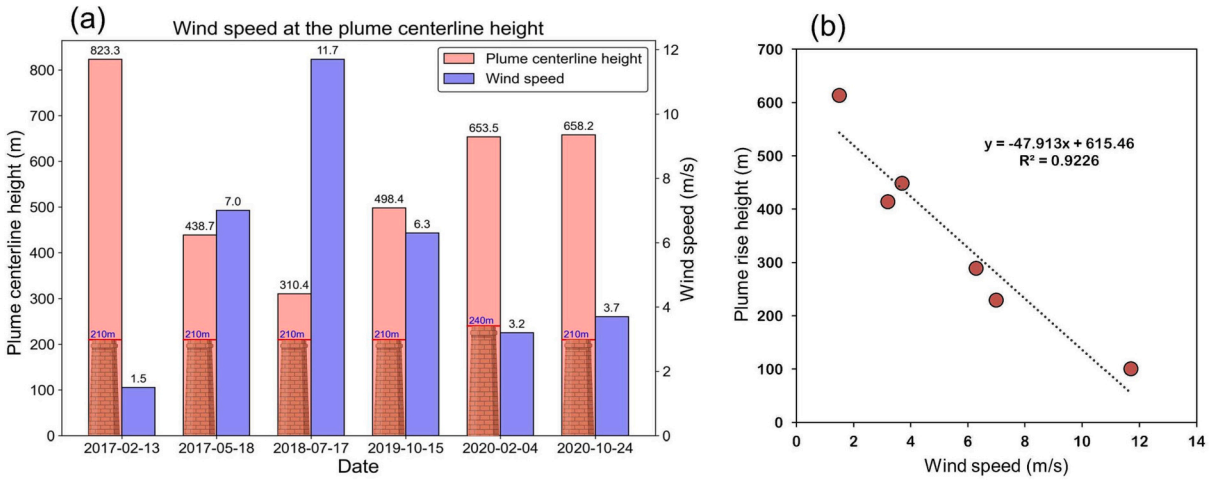

Fig. 2. (a) Simulated plume centerline height and wind speed at the plume centerline height for the 6 cases, and (b) the relationship between plume rise height and wind speed.

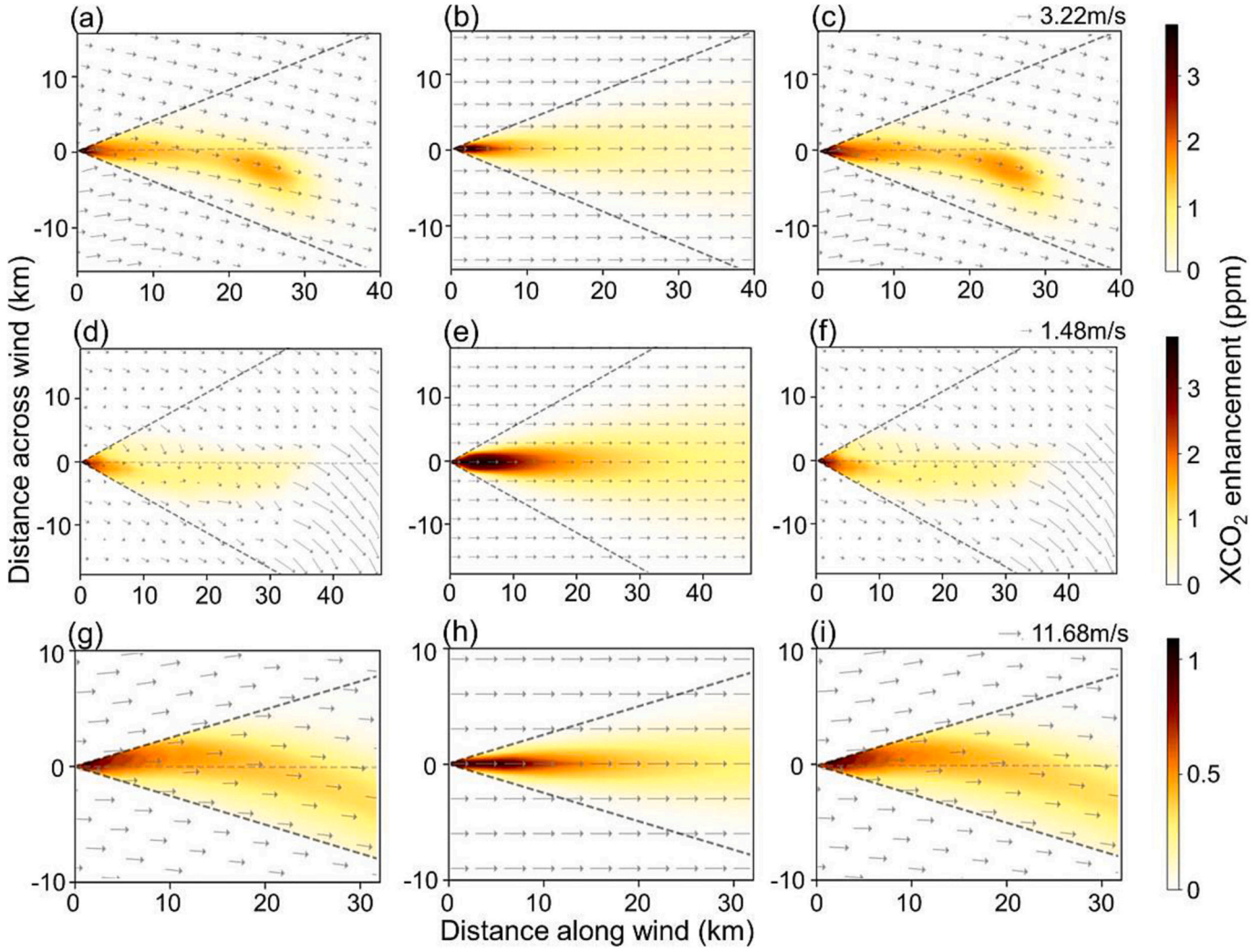

Fig. 3. Simulated XCO_2 enhancement distributions with prior emissions of 25 $ktCO_2$/day for cases on (a, b, c) 2020-02-04, (d, e, f) 2017-02-13, and (g, h, i) 2018-07-17. (a, d, g) CMAQ weighted XCO_2 enhancement, (b, e, h) Gaussian plume model XCO_2 enhancement, and (c, f, i) CMAQ averaged XCO_2 enhancement, respectively.

lower than that on 2017-02-13. This is most likely caused by the accelerated diffusion of CO_2 due to excessive wind speed, which is similar to 2017-05-18 and 2019-10-15 cases (Fig. S3 and Fig. S4). On 2020-10-24 (Fig. S2), the wind speed was moderate and the XCO_2 at the power plant location was also moderate among the 6 cases. In addition, it also shows that the XCO_2 enhancement of the GPM plumes is

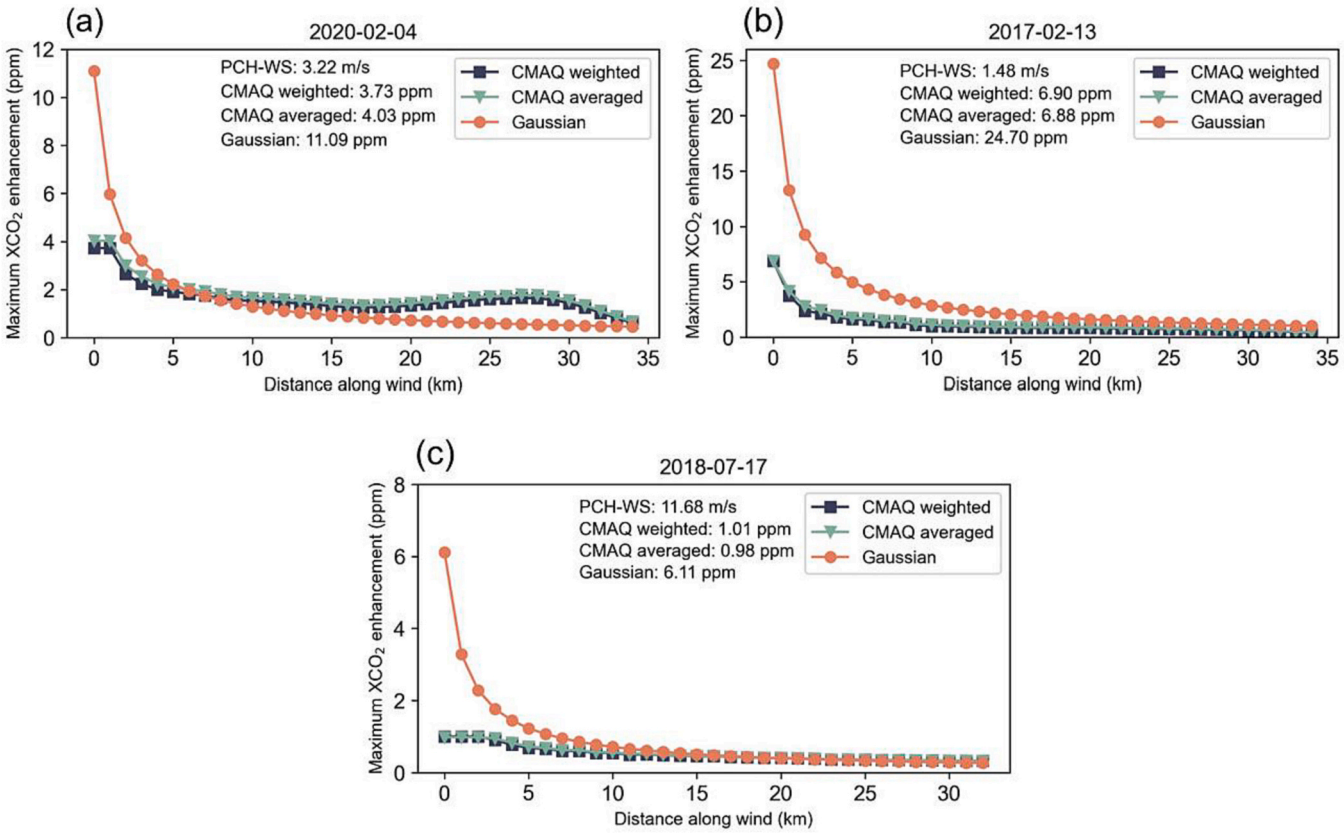

Fig. 4. Maximum XCO_2 enhancement along the wind direction simulated with prior emissions of 25 $ktCO_2$/day for cases on (a) 2020-02-04, (b) 2017-02-13, and (c) 2018-07-17.

significantly higher than the CMAQ weighted/averaged plumes within 0–5 km from the power plants. This is due to the fact that in the CMAQ simulation, after CO_2 is discharged from the stack opening, it also diffuses in all directions and is transported downwind as it rises, resulting in lower XCO_2 concentrations in the vicinity of the stack opening (Fig. S5), whereas the GPM simulation assumes that CO_2 is discharged along the dominant wind direction at the plume centerline height, resulting in much higher XCO_2 concentrations downwind of the stack. On 2018-07-17 (Fig. 4(c)), after 20 km away from the stack, the XCO_2 concentrations of CMAQ and GPM plumes were roughly similar. These are also reflected in other cases (Fig. S2(d), S3(d) and S4(d)) and commonly indicate that if the satellite observation is within 0–5 km of the power plant, the emission estimation of GPM will be significantly lower than that of CMAQ; and if the satellite observation is located about 20 km away from the power plant, the estimated emissions using GPM and CMAQ will be closer except for some cases with plume landing point. In addition, it also could be found that the XCO_2 calculated with the weighting method is slightly lower than the column-averaged XCO_2, with a difference of about 0.1 ppm, indicating that the traditional used GPM combined with column averaging to obtain XCO_2 also leads to an underestimation of the inverted emissions.

3.3. Estimated emissions

The estimated CO_2 emission results for the 6 cases are summarized in Table 2. The reported daily emissions of each power plant are also shown in Table 2, converted from the annual emissions available on the Carbon Brief website (https://www.carbonbrief.org/mapped-worlds-coal-power-plants). The Carbon Brief analysis shows the world's coal-fired power plants operating between 2000 and 2019, which was compiled using the data from Global Energy Monitor and Global Coal Plant Tracker. It includes approximately 2465 power plants in China,

Table 2
Estimated emissions for the 6 cases (unit: $ktCO_2$/day).

Date	Name	GPM	CMAQ weight	CMAQ average	Reported values
2017/2/13	Shanghai Wujing Power Station	15.5 ± 11.0	44.9 ± 32.2	41.0 ± 30.0	32.7
2017/5/18	Jiangsu Nantong Power Station	64.0 ± 12.4	77.1 ± 15.7	74.7 ± 15.1	33.1
2018/7/17	Zhejiang Jiaxing Power Station	116.0 ± 15.7	145.6 ± 25.1	141.1 ± 24.0	61.7
2019/10/15	Guoneng Tongling Power Station	41.0 ± 12.2	80.1 ± 27.4	79.6 ± 27.3	14.8
2020/2/4	Guohua Taicang Power Station	96.7 ± 38.2	45.1 ± 18.8	44.2 ± 18.4	42.8
2020/10/24	Huadian Jurong Power Station	21.0 ± 7.4	45.1 ± 16.7	41.4 ± 15.4	44.4

with the installed capacity ranging from 30 MW to 6720 MW, of which 1033 plants have CO_2 emissions greater than 10 $ktCO_2$/day. The GPM estimated results are almost 2 or 0.5 times the reported emissions. On 2020-02-04 and 2020-10-24, the CMAQ estimated emissions are very close to the reported emissions, while all the remaining cases are higher than the reported. The difference of emission estimations between GPM and CMAQ averaged is 15–90 %, and the difference between CMAQ weighted and CMAQ averaged is 1–9 %. On 2020-02-04, the CMAQ plume landing site appeared at about 20 km, where the OCO-2 satellite passed, so the CMAQ estimation result is much closer to the reported than GPM, which doesn't have the potential to simulate the plume landing site. On 2017-02-13 and 2020-10-24, when the wind speeds were relatively low, the distances between the power plant stack locations and OCO-2 soundings were 1.5 km and 2.8 km, respectively, so the

GPM modeled XCO_2 were higher, and the GPM estimations are all lower than the reported. According, the emissions estimated from the CMAQ simulations are much higher than those from GPM, and have better consistency with the reported values. On 2017-05-18, the distance between the power plant stack location and OCO-2 soundings was 3.6 km, which is also within 5 km. CMAQ XCO_2 is lower than GPM, and the estimated emission using CMAQ is higher than that using GPM. Nevertheless, the estimated emissions from both CMAQ and GPM are significantly higher than the reported, which may be related to the simulation error of wind speed at the plume rise height. We evaluated the simulated upper air wind speeds of D03 against the meteorological sounding observations (Fig. 1). On that day, the simulated wind speed is overestimated by 1.0 m/s, resulting in lower simulated XCO_2 and significantly overestimated emissions. Similarly, on 2018-07-17 and 2019-10-15, the simulated wind speeds are overestimated by 2.0 and 1.2 m/s, respectively (Table S1), accordingly, the estimates from both the GPM and CMAQ model are significantly higher than the reported values. These indicate that on the one hand, the CMAQ inline plume simulation could significantly improve the CO_2 emissions from power plants, and on the other hand, the estimation is very sensitive to the wind speed simulations, although we use a better plume model, the simulation bias in wind speed can significantly affect the inversion results.

It is easy to change the wind speed in the GPM model, and we attempted to investigate the effect of wind speed on emission inversion. After increasing/decreasing the wind speed by 1 m/s, we found that the CO_2 emission rate of the power plants can increase/decrease in the range of 5.62 to 30.03 $ktCO_2$/day. The XCO_2 calculation method has a much smaller effect on the inversion results compared to other factors. Compared with the weighted method, the emissions estimated based on the column averaged XCO_2 will be underestimated in the range of 1–9 %. It is worth noting that the CMAQ averaged is similar to the GPM XCO_2. It's just that the GPM XCO_2 does not take into account the pressure variation, and the surface density is the same in every plane of the air column, so the CO_2 molecules are equally distributed in the air column. The setting of the a priori emission rate and the use of different versions of the OCO-2 XCO_2 product can also affect the inversion results. Therefore, we performed additional experiments with an a priori value of 50 $ktCO_2$/day and using OCO-2 XCO_2 ACOS v11 retrievals. The results show that for the GPM model, the use of different a priori values has no effect on the inversion results, while for the CMAQ model, doubling the a priori value only slightly reduces the inverted carbon emissions by about 2 % (Table S3), which is negligible compared to the difference between the inversion results using the GPM and CMAQ models. The version of OCO-2 XCO_2 retrievals has a noticeable effect on the estimated emissions, with the use of the v11 version data leading to changes in the inverted emissions ranging from −10 % to 13 %, and in general the results of the inversion being slightly closer to the reported values. However, the differences caused by the version of XCO_2 are still much smaller than those caused by the GPM and CMAQ models (Table S4).

4. Summary and conclusion

In this study, based on the OCO-2 XCO_2 retrievals over YRD, China, we use the GPM and WRF-CMAQ model to simulate the CO_2 plumes of 6 power plants, and estimate the CO_2 emissions. We analyze the differences in simulated CO_2 plumes and estimated CO_2 emissions using different models, and also, explore the impact of different XCO_2 calculation methods on the emission estimates.

The results show that the differences in estimated emissions between CMAQ and GPM are in the range of 15–90 %. If the satellite observations are within 0–5 km away from the power plant, the emission estimated based on the GPM simulations is much lower than the one estimated based on the CMAQ simulations. After 20 km, the emissions estimated based on both GPM and CMAQ simulations are close. Compared with the reported emission values, the CO_2 emissions based on the GPM simulations can be significantly overestimated or underestimated, while the CMAQ inline plume simulation could significantly improve the estimates. Moreover, the accuracy of wind speed can significantly affect the estimates of CO_2 emissions in both the GPM and CMAQ simulations, with the higher wind speed resulting in lower XCO_2 simulations and higher CO_2 emission estimations. The influence of the different XCO_2 calculation ways is small, with a relative change of about 1–9 %.

Our findings indicate that accurate meteorological field and plume simulations are critical for future point source emission inversions. For the meteorological field, although we used a state-of-the-art mesoscale meteorological model to simulate the wind field at 1 km horizontal resolution, the simulated wind speeds are still subject to varying degrees of bias. Techniques such as data assimilation may be required in the future to further improve the simulation of the wind field.

CRediT authorship contribution statement

Yingsong Li: Data curation, Investigation, Methodology, Software, Validation, Visualization, Writing – original draft, Writing – review & editing. **Fei Jiang:** Conceptualization, Methodology, Validation, Writing – review & editing. **Mengwei Jia:** Data curation, Software. **Shuzhuang Feng:** Data curation, Software. **Yong Lai:** Data curation. **Junnan Ding:** Data curation. **Wei He:** Writing – review & editing. **Hengmao Wang:** Writing – review & editing. **Mousong Wu:** Writing – review & editing. **Jun Wang:** Writing – review & editing. **Fanhui Shen:** Data curation. **Lingyu Zhang:** Writing – review & editing.

Declaration of competing interest

The authors declare that they have no known competing financial interests or personal relationships that could have appeared to influence the work reported in this paper.

Data availability

Data will be made available on request.

Acknowledgments

This work is supported by the National Key Research and Development Program of China (Grant 2021YFB3901001), and the National Natural Science Foundation of China (Grants 42377102 and 72293603). The authors also gratefully acknowledge the High-Performance Computing Center (HPCC) of Nanjing University for performing the numerical calculations in this paper on its blade cluster system.

Appendix A. Supplementary data

Supplementary data to this article can be found online at https://doi.org/10.1016/j.scitotenv.2023.169586.

References

Bieser, J., Aulinger, A., Matthias, V., Quante, M., Denier van der Gon, H.A., 2011. Vertical emission profiles for Europe based on plume rise calculations. Environ. Pollut. 159, 2935–2946. https://doi.org/10.1016/j.envpol.2011.04.030.

Bovensmann, H., Buchwitz, M., Burrows, J.P., Reuter, M., Krings, T., Gerilowski, K., Schneising, O., Heymann, J., Tretner, A., Erzinger, J., 2010. A remote sensing technique for global monitoring of power plant CO_2 emissions from space and related applications. Atmos. Meas. Tech. 3, 781–811. https://doi.org/10.5194/amt-3-781-2010.

Broquet, G., Bréon, F.-M., Renault, E., Buchwitz, M., Reuter, M., Bovensmann, H., Chevallier, F., Wu, L., Ciais, P., 2018. The potential of satellite spectro-imagery for monitoring CO_2 emissions from large cities. Atmos. Meas. Tech. 11, 681–708. https://doi.org/10.5194/amt-11-681-2018.

Brunner, D., Kuhlmann, G., Marshall, J., Clément, V., Fuhrer, O., Broquet, G., Löscher, A., Meijer, Y., 2019. Accounting for the vertical distribution of emissions in atmospheric

CO_2 simulations. Atmos. Chem. Phys. 19, 4541–4559. https://doi.org/10.5194/acp-19-4541-2019.

Brunner, D., Kuhlmann, G., Henne, S., Koene, E., Kern, B., Wolff, S., Voigt, C., Jöckel, P., Kiemle, C., Roiger, A., Fiehn, A., Krautwurst, S., Gerilowski, K., Bovensmann, H., Borchardt, J., Galkowski, M., Gerbig, C., Marshall, J., Klonecki, A., Prunet, P., Hanfland, R., Pattantyús-Ábrahám, M., Wyszogrodzki, A., Fix, A., 2023. Evaluation of simulated CO_2 power plant plumes from six high-resolution atmospheric transport models. Atmos. Chem. Phys. 23, 2699–2728. https://doi.org/10.5194/acp-23-2699-2023.

Brusca, S., Famoso, F., Lanzafame, R., Mauro, S., Garrano, A.M.C., Monforte, P., 2016. Theoretical and experimental study of Gaussian plume model in small scale system. Energy Procedia 101, 58–65. https://doi.org/10.1016/j.egypro.2016.11.008.

Connor, B.J., Boesch, H., Toon, G., Sen, B., Miller, C., Crisp, D., 2008. Orbiting carbon observatory: inverse method and prospective error analysis. J. Geophys. Res. 113, D05305. https://doi.org/10.1029/2006jd008336.

Eldering, A., O'Dell, C.W., Wennberg, P.O., Crisp, D., Gunson, M.R., Viatte, C., Avis, C., Braverman, A., Castano, R., Chang, A., Chapsky, L., Cheng, C., Connor, B., Dang, L., Doran, G., Fisher, B., Frankenberg, C., Fu, D., Granat, R., Hobbs, J., Lee, R.A.M., Mandrake, L., McDuffie, J., Miller, C.E., Myers, V., Natraj, V., O'Brien, D., Osterman, G.B., Oyafuso, F., Payne, V.H., Pollock, H.R., Polonsky, I., Roehl, C.M., Rosenberg, R., Schwandner, F., Smyth, M., Tang, V., Taylor, T.E., To, C., Wunch, D., Yoshimizu, J., 2017. The Orbiting Carbon Observatory-2: first 18 months of science data products. Atmos. Meas. Tech. 10, 549–563. https://doi.org/10.5194/amt-10-549-2017.

Friedlingstein, P., O'Sullivan, M., Jones, M.W., Andrew, R.M., Gregor, L., Hauck, J., Le Quéré, C., Luijkx, I.T., Olsen, A., Peters, G.P., Peters, W., Pongratz, J., Schwingshackl, C., Sitch, S., Canadell, J.G., Ciais, P., Jackson, R.B., Alin, S.R., Alkama, R., Arneth, A., Arora, V.K., Bates, N.R., Becker, M., Bellouin, N., Bittig, H.C., Bopp, L., Chevallier, F., Chini, L.P., Cronin, M., Evans, W., Falk, S., Feely, R.A., Gasser, T., Gehlen, M., Gkritzalis, T., Gloege, L., Grassi, G., Gruber, N., Gürses, Ö., Harris, I., Hefner, M., Houghton, R.A., Hurtt, G.C., Iida, Y., Ilyina, T., Jain, A.K., Jersild, A., Kadono, K., Kato, E., Kennedy, D., Klein Goldewijk, K., Knauer, J., Korsbakken, J.I., Landschützer, P., Lefèvre, N., Lindsay, K., Liu, J., Liu, Z., Marland, G., Mayot, N., McGrath, M.J., Metzl, N., Monacci, N.M., Munro, D.R., Nakaoka, S.-I., Niwa, Y., O'Brien, K., Ono, T., Palmer, P.I., Pan, N., Pierrot, D., Pocock, K., Poulter, B., Resplandy, L., Robertson, E., Rödenbeck, C., Rodriguez, C., Rosan, T.M., Schwinger, J., Séférian, R., Shutler, J.D., Skjelvan, I., Steinhoff, T., Sun, Q., Sutton, A.J., Sweeney, C., Takao, S., Tanhua, T., Tans, P.P., Tian, X., Tian, H., Tilbrook, B., Tsujino, H., Tubiello, F., van der Werf, G.R., Walker, A.P., Wanninkhof, R., Whitehead, C., Willstrand Wranne, A., Wright, R., Yuan, W., Yue, C., Yue, X., Zaehle, S., Zeng, J., Zheng, B., 2022. Global carbon budget 2022. Earth Syst. Sci. Data 14, 4811–4900. https://doi.org/10.5194/essd-14-4811-2022.

Gao, M., Carmichael, G.R., Wang, Y., Ji, D., Liu, Z., Wang, Z., 2016. Improving simulations of sulfate aerosols during winter haze over Northern China: the impacts of heterogeneous oxidation by NO_2. Front. Environ. Sci. Eng. 10, 16. https://doi.org/10.1007/s11783-016-0878-2.

Guevara, M., Soret, A., Arévalo, G., Martínez, F., Baldasano, J.M., 2014. Implementation of plume rise and its impacts on emissions and air quality modelling. Atmos. Environ. 99, 618–629. https://doi.org/10.1016/j.atmosenv.2014.10.029.

Guo, W., Shi, Y., Liu, Y., Su, M., 2023. CO_2 emissions retrieval from coal-fired power plants based on OCO-2/3 satellite observations and a Gaussian plume model. J. Clean. Prod. 397 https://doi.org/10.1016/j.jclepro.2023.136525.

Houyoux, M., 1998. Technical Report: Plume Rise Algorithm Summary for the Sparse Matrix Operator Modeling System (SMOKE).Prepared for North Carolina Department of Environment and Natural Resources. UNC, Chapel Hill, North Carolina. ENV 98TR004eTR0v1.0.

Hu, Y., Shi, Y., 2021. Estimating CO_2 emissions from large scale coal-fired power plants using OCO-2 observations and emission inventories. Atmosphere 12 (7), 811. https://doi.org/10.3390/atmos12070811.

Johnson, M.S., Schwandner, F.M., Potter, C.S., Nguyen, H.M., Bell, E., Nelson, R.R., Philip, S., O'Dell, C.W., 2020. Carbon dioxide emissions during the 2018 Kilauea volcano eruption estimated using OCO-2 satellite retrievals. Geophys. Res. Lett. 47 https://doi.org/10.1029/2020gl090507 e2020GL090507.

Lei, R., Feng, S., Danjou, A., Broquet, G., Wu, D., Lin, J.C., O'Dell, C.W., Lauvaux, T., 2021. Fossil fuel CO_2 emissions over metropolitan areas from space: a multi-model analysis of OCO-2 data over Lahore, Pakistan. Remote Sens. Environ. 264, 112625 https://doi.org/10.1016/j.rse.2021.112625.

Lei, R., Feng, S., Xu, Y., Tran, S., Ramonet, M., Grutter, M., Garcia, A., Campos-Pineda, M., Lauvaux, T., 2022. Reconciliation of asynchronous satellite-based NO_2 and XCO_2 enhancements with mesoscale modeling over two urban landscapes. Remote Sens. Environ. 281, 113241 https://doi.org/10.1016/j.rse.2022.113241.

Lin, X., van der A, R., de Laat, J., Eskes, H., Chevallier, F., Ciais, P., Deng, Z., Geng, Y., Song, X., Ni, X., Huo, D., Dou, X., Liu, Z., 2023. Monitoring and quantifying CO_2 emissions of isolated power plants from space. Atmos. Chem. Phys. 23, 6599–6611. https://doi.org/10.5194/acp-23-6599-2023.

Nassar, R., Hill, T.G., McLinden, C.A., Wunch, D., Jones, D.B.A., Crisp, D., 2017. Quantifying CO_2 emissions from individual power plants from space. Geophys. Res. Lett. 44, 10045–10053. https://doi.org/10.1002/2017gl074702.

Nassar, R., Mastrogiacomo, J.-P., Bateman-Hemphill, W., McCracken, C., MacDonald, C. G., Hill, T., O'Dell, C.W., Kiel, M., Crisp, D., 2021. Advances in quantifying power plant CO_2 emissions with OCO-2. Remote Sens. Environ. 264, 112579 https://doi.org/10.1016/j.rse.2021.112579.

Ng, H.L., Hashim, M., 2023. Mapping trends of carbon dioxide and methane during movement control order in industrial areas in Peninsular Malaysia using GOSAT, GOSAT-2, OCO-2, OCO-3, and TROPOMI satellites data. In: Int. Arch. Photogramm. Remote Sens. Spatial Inf. Sci., XLVIII-4/W6-2022, pp. 273–278. https://doi.org/10.5194/isprs-archives-XLVIII-4-W6-2022-273-2023.

O'Dell, C.W., Connor, B., Bösch, H., O'Brien, D., Frankenberg, C., Castano, R., Christi, M., Eldering, D., Fisher, B., Gunson, M., McDuffie, J., Miller, C.E., Natraj, V., Oyafuso, F., Polonsky, I., Smyth, M., Taylor, T., Toon, G.C., Wennberg, P.O., Wunch, D., 2012. The ACOS CO_2 retrieval algorithm — part 1: description and validation against synthetic observations. Atmos. Meas. Tech. 5, 99–121. https://doi.org/10.5194/amt-5-99-2012.

Ooi, M.C.-G., Chuang, M.-T., Fu, J.S., Kong, S.S., Huang, W.-S., Wang, S.-H., Pimonsree, S., Chan, A., Pani, S.K., Lin, N.-H., 2021. Improving prediction of trans-boundary biomass burning plume dispersion: from northern peninsular Southeast Asia to downwind western North Pacific Ocean. Atmos. Chem. Phys. 21, 12521–12541. https://doi.org/10.5194/acp-21-12521-2021.

Pillai, D., Buchwitz, M., Gerbig, C., Koch, T., Reuter, M., Bovensmann, H., Marshall, J., Burrows, J.P., 2016. Tracking city CO_2 emissions from space using a high-resolution inverse modelling approach: a case study for Berlin, Germany. Atmos. Chem. Phys. 16, 9591–9610. https://doi.org/10.5194/acp-16-9591-2016.

Razmjoo, A., Gakenia Kaigutha, L., Vaziri Rad, M.A., Marzband, M., Davarpanah, A., Denai, M., 2021. A technical analysis investigating energy sustainability utilizing reliable renewable energy sources to reduce CO_2 emissions in a high potential area. Renew. Energy 164, 46–57. https://doi.org/10.1016/j.renene.2020.09.042.

Schwandner, F.M., Gunson, M.R., Miller, C.E., Carn, S.A., Eldering, A., Krings, T., Verhulst, K.R., Schimel, D.S., Nguyen, H.M., Crisp, D., O'Dell, C.W., Osterman, G.B., Iraci, L.T., Podolske, J.R., 2017. Spaceborne detection of localized carbon dioxide sources. Science 358, eaam5782. https://doi.org/10.1126/science.aam5782.

Skamarock, W.C., Klemp, J.B., Dudhia, J., Gill, D.O., Liu, Z., Berner, J., Wang, W., Powers, J.G., Duda, M.G., Barker, D.M., 2019. A description of the advanced research WRF model version 4. Natl. Cent. Atmosph. Res. 145 https://doi.org/10.5065/1dfh-6p97. Boulder, CO, USA.

United States Environmental Protection Agency, 2014. CMAQv5.0.2, Version 5.0.2. https://doi.org/10.5281/zenodo.1079898. Zenodo.

Varon, D.J., Jacob, D.J., McKeever, J., Jervis, D., Durak, B.O.A., Xia, Y., Huang, Y., 2018. Quantifying methane point sources from fine-scale satellite observations of atmospheric methane plumes. Atmos. Meas. Tech. 11, 5673–5686. https://doi.org/10.5194/amt-11-5673-2018.

Ye, X., Lauvaux, T., Kort, E.A., Oda, T., Feng, S., Lin, J.C., Yang, E.G., Wu, D., 2020. Constraining fossil fuel CO_2 emissions from urban area using OCO-2 observations of total column CO_2. J. Geophys. Res.-Atmos. 125 https://doi.org/10.1029/2019JD030528 e2019JD030528.

Yoro, K.O., Daramola, M.O., 2020. CO_2 emission sources, greenhouse gases, and the global warming effect. In: Advances in Carbon Capture, pp. 3–28.

Zhang, L., Gong, S., Zhao, T., Zhou, C., Wang, Y., Li, J., Ji, D., He, J., Liu, H., Gui, K., Guo, X., Gao, J., Shan, Y., Wang, H., Wang, Y., Che, H., Zhang, X., 2021. Development of WRF/CUACE v1.0 model and its preliminary application in simulating air quality in China. Geosci. Model Dev. 14, 703–718. https://doi.org/10.5194/gmd-14-703-2021.

Zheng, B., Chevallier, F., Ciais, P., Broquet, G., Wang, Y., Lian, J., Zhao, Y., 2020. Observing carbon dioxide emissions over China's cities and industrial areas with the Orbiting Carbon Observatory-2. Atmos. Chem. Phys. 20, 8501–8510. https://doi.org/10.5194/acp-20-8501-2020.

Zheng, T., Nassar, R., Baxter, M., 2019. Estimating power plant CO_2 emission using OCO-2 XCO_2 and high resolution WRF-Chem simulations. Environ. Res. Lett. 14, 085001 https://doi.org/10.1088/1748-9326/ab25ae.